# Energy Conversion within Current Sheets in the Earth's Quasi-parallel Magnetosheath

Steven J. Schwartz[1], Harald Kucharek[2], Charles J Farrugia[2], Karlheinz Trattner[3], Imogen Gingell[4], Robert E Ergun[5], Robert J. Strangeway[6], and Daniel J Gershman[7]

[1]University of Colorado Boulder
[2]University of New Hampshire, USA
[3]Laboratory for Atmospheric and Space Physics
[4]School of Physics and Astronomy, University of Southampton
[5]Univeristy of Colorado
[6]University of California Los Angeles
[7]NASA Goddard Space Flight Center

November 21, 2022

**Abstract**

Shock waves in collisionless plasmas rely on kinetic processes to convert the primary incident bulk flow energy into thermal energy. That conversion is initiated within a thin transition layer but may continue well into the downstream region. At the Earth's bow shock, the region downstream of shock locations where the interplanetary magnetic field is nearly parallel to the shock normal is highly turbulent. We study the distribution of thin current events in this magnetosheath. Quantification of the energy dissipation rate made by the MMS spacecraft shows that these isolated intense currents are distributed uniformly throughout the magnetosheath and convert a significant fraction (5%-11%) of the energy flux incident at the bow shock.

# Energy Conversion within Current Sheets in the Earth's Quasi-parallel Magnetosheath

**Steven J Schwartz[1*†], Harald Kucharek[2], Charles J Farrugia[2], K.J. Trattner[1], Imogen Gingell[3], Robert Ergun[1], Robert Strangeway[4], Daniel Gershman[5]**

[1]Laboratory for Atmospheric and Space Physics, CU Boulder, Boulder, CO
[2]University of New Hampshire, Durham, NH
[3]Physics and Astronomy, University of Southampton, Southampton, UK
[4]UCLA, Los Angeles, CA
[5]Goddard Space Flight Center, Greenbelt, MD

**Key Points:**

- Intense current events are distributed uniformly downstream of a quasi-parallel bow shock.
- The events are associated primarily with a conversion of field energy into particle energy.
- The energy processed by these events is a non-negligible fraction of the energy incident at the bow shock.

Manuscript Date 11/24/2020

*Laboratory for Atmospheric and Space Physics, CU Boulder, Boulder, CO
†Also Emeritus Professor, Imperial College London

Corresponding author: Steven Schwartz, `steven.schwartz@lasp.colorado.edu`

**Abstract**

Shock waves in collisionless plasmas rely on kinetic processes to convert the primary incident bulk flow energy into thermal energy. That conversion is initiated within a thin transition layer but may continue well into the downstream region. At the Earth's bow shock, the region downstream of shock locations where the interplanetary magnetic field is nearly parallel to the shock normal is highly turbulent. We study the distribution of thin current events in this magnetosheath. Quantification of the energy dissipation rate made by the MMS spacecraft shows that these isolated intense currents are distributed uniformly throughout the magnetosheath and convert a significant fraction (5%-11%) of the energy flux incident at the bow shock.

## Plain Language Summary

Shock waves form when a supersonic flow encounters an immovable object. Thus, ahead of the magnetic bubble formed by the Earth's extended magnetic field, the flow of charged particles emanating from the Sun known as the solar wind is shocked, slowed, and deflected around the Earth. In dense fluids, the conversion of the incident bulk flow energy into heat is accomplished by collisions between particles or molecules. However, the solar wind is so rarefied that such collisions are negligible, and the energy conversion involves more than one kinetic process that couples the different particles to the electromagnetic fields. Under some orientations of the interplanetary magnetic field carried by the wind, the shocked medium is highly turbulent. Within that turbulence are isolated thin regions carrying large electric currents. We have studied those currents, and find that they are converting energy from one form to another at a rate that is a significant fraction of the incident energy flux. Thus, these currents contribute significantly to the overall shock energetics.

## 1 Introduction

Shock waves in astrophysical plasma are almost always operating on scales that are much smaller than the particle collisional mean free path. Such collisionless shocks require plasma kinetic processes to decelerate the dominant incident bulk flow and "dissipate" that incident energy flux. These processes operate differently on the different plasma species and electromagnetic fields, and over different scales. They are responsible for preferential heating together with the acceleration to high energies of sub-populations of particles (Kucharek et al., 2003). The bow shock formed by the interaction of the supersonic solar wind flow with the Earth's magnetosphere has long been a prime laboratory for investigating collisionless shock physics thanks to its accessibility by ever-increasing high quality in situ satellite observations (Burgess & Scholer, 2015; Schwartz, 2006; Schwartz et al., 2013; Krasnoselskikh et al., 2013; Tsurutani & Stone, 1985; Stone & Tsurutani, 1985; Scudder et al., 1986).

The orientation of the upstream (unshocked) magnetic field plays a critical role in the physics of collisionless shocks. At quasi-parallel shocks, in which the angle $\theta_{Bn}$ between that field and the vector normal to the shock is less than 45°, the particle gyration around the magnetic field is unable to confine particles on the scale of their Larmor radii due to their mobility parallel to the field. The result is an extended "foreshock" region (Eastwood et al., 2005) where backstreaming particles drive instabilities that result in large-amplitude magnetic disturbances and attendant accelerated particles.

The region downstream of the quasi-parallel shock (Burgess et al., 2005) is also much more turbulent than that behind a quasi-perpendicular shock. This quasi-parallel magnetosheath is of interest for several reasons. Firstly, recent work by Matthaeus et al. (2020) has considered it from the perspective of fundamental turbulence, comparing the turbulence spectrum and properties to the fully developed turbulence found in solar wind. The sheath turbulence is somewhat intermittent, implying that there are coherent structures embedded within it. They re-cast the energy equations, isolating terms via their so-called "$\Pi - D$" formulation to distinguish reversible energy exchange, such as adiabatic compression, from irreversible dissipation. They do not find any strong correlation between that dissipation and, e.g., regions of intense currents.

Retinò et al. (2007) reported early evidence of localized current sheets that were in the process of magnetically reconnecting. In the context of turbulence in collisionless plasmas, reconnection is thought to be a possible mechanism for the dissipation of energy that has cascaded from larger scales down to kinetic scales. Magnetic reconnection also relaxes the field topology as it heats or accelerates the particles. More recently, using high-resolution data from the Magnetospheric Multiscale (MMS) mission, Phan et al. (2018) found examples in the magnetosheath of reconnecting current sheets at small, electron scales in which only the electrons participate in the reconnection process. This work highlights the electron-only microphysics within complex turbulent environments.

By contrast, reconnection on larger scales associated with macroscopic boundaries and topological changes, such as that at the magnetopause, results in ion acceleration and jets at scales larger than the electron diffusion region. Ongoing work, (e.g, Wilder et al., 2018; Stawarz et al., 2019), has pursued the reconnection process, associated turbulence and statistics within the magnetosheath.

Gingell et al. (2019) found small-scale reconnection events within the transition layer at a quasi-parallel shock in both MMS data and simulation results. Wang et al. (2019) and Bessho et al. (2020) have extended these results to other shock geometries. These current sheets appear to be localized at/near the shock itself (Gingell et al., 2020) and are believed to represent a collisionless mechanism that contributes to the overall shock dissipation and field topology relaxation, driving the system toward a more homogeneous equilibrium plasma state.

To date, there has not been a comprehensive study of the specific role of thin current structures in energy re-distribution throughout the magnetosheath. This is clearly related to the turbulence laboratory that this region of geospace offers. However, here we focus on the fact that the magnetosheath represents the downstream state of the bow shock, and a state that is still far from the uniform thermal equilibrium of textbook shocks in collisional fluids. We shall address the question: What role do small intense current structures downstream of the quasi-parallel shock play in the overall shock energetics? We address this question through a relatively unique volume of burst mode data taken during a single traversal of the sub-solar magnetosheath by the MMS spacecraft.

The next section summarizes both the data and our primary analysis methods. We then present our Results and provide some Discussion before drawing our final Conclusions.

## 2 Data and Methodology

Our primary results are drawn from the Magnetospheric Multiscale mission (MMS) (Burch, Moore, et al., 2016). We also used data from both the Wind and Artemis spacecraft to establish the prevailing interplanetary conditions. An overview of the traversal of the terrestrial magnetosheath is shown in Figure 1, with the burst-mode data expanded in Figure 2. The analysis relies on data from the Fast Plasma Investigation (FPI) (Pollock et al., 2016), Fluxgate Magnetometer (FGM) (Russell et al., 2016) and electric field instrumentation (Torbert et al., 2016; Ergun et al., 2016; Lindqvist et al., 2016). We will concentrate on the latter half of this outbound traversal which corresponds to conditions behind the quasi-parallel shock under steady interplanetary conditions (see Figure 1g and Figure S1 in the Supporting Information). The MMS trajectory was nearly radial and encountered the bow shock close to the sub-solar point (Figure 1h). Figure 1 shows that the quasi-parallel magnetosheath is highly turbulent, and that there is ongoing deceleration, compression and heating with distance behind the bow shock. Fortuitously, MMS burst mode data are available almost continuously (see Figure 2) throughout this encounter with the turbulent quasi-parallel sheath region.

[Figure 1 about here.]

The solar wind parameters deduced from Wind (see Figure S1 of the Supporting Information) are: number density $n = 3.34\text{cm}^{-3}$, proton and electron temperatures $T_p = 4.55\text{eV}$, $T_e = 13.9\text{eV}$, speed $V_{sw} = 400\text{km/s}$, and average GSE magnetic field vector $\mathbf{B} = (4.08, 1, 51, 0.079)\text{nT}$ with $|\mathbf{B}| = 4.35\text{nT}$. The normal to the bow shock, found by scaling a model bow shock (Slavin & Holzer, 1981; Schwartz, 1998) to the MMS crossing, was $(0.993, 0.036, 0.111)$GSE, reflecting the location very near to the sub-solar point. These values lead to a plasma $\beta = 1.3$, an Alfvén mach number of 7.7 and a fast magnetosonic mach number of 6.5. The shock geometry was $\theta_{Bn} \sim 19°$.

We use the curlometer four-spacecraft method (Chanteur, 1998; Dunlop & Eastwood, 2008) to determine the electric current density $\mathbf{j}$. We take advantage of the 30 ms FPI electron measurements to compute the electric field $\mathbf{E}' = \mathbf{E} + \mathbf{v}_e \times \mathbf{B}$ in the electron rest frame smoothed to match the 30 ms electron cadence, where $\mathbf{v}_e$ is the bulk electron fluid velocity and $\mathbf{B}$ is the magnetic field. We calculate $\mathbf{E}'$ at the barycenter of the tetrahedron by combining data from the four spacecraft, to match the curlometer estimation of $\mathbf{j}$. We then calculate the energy conversion (Swisdak et al., 2018) between fields and particles, namely $\mathbf{j} \cdot \mathbf{E}'$. Positive values of $\mathbf{j} \cdot \mathbf{E}'$ correspond to energy conversion from the fields to the particles. Note that, apart from the lower cadence of the data, employing the ion velocity instead of $\mathbf{v}_e$ will lead to the same energy transfer rate, as the difference between the two expressions is $\mathbf{j} \cdot (\mathbf{v}_i - \mathbf{v}_e) \times \mathbf{B} \propto \mathbf{j} \cdot \mathbf{j} \times \mathbf{B} = \mathbf{0}$ in a singly ionized plasma (Zenitani et al., 2011). Other MMS data shown are drawn from MMS1.

[Figure 2 about here.]

Our event selection identifies instances of high current densities, specifically ones in which the magnitudes are $3\sigma$ above the average for the entire interval. We then select manually the region surrounding that peak in $\mathbf{j}$ that captures the full current structure. One such example in shown in Figure 3. The Supporting Information includes similar plots for all 59 events. This event displays a near magnetic null coincident with a reversal in the $B_y$ component, reminiscent of reconnecting current sheets (Burch, Torbert, et al., 2016). There is a rise in the particle pressures (panel g) due primarily to a rise in density (not shown), as the ion temperature decreases there. Total pressure balance is maintained across the event. There is a clear signature in $\mathbf{j}\cdot\mathbf{E}'$ (panel e) which is much reduced outside the event even where there are significant current and field values. We are primarily interested in the contribution of these events to the energy budget mediated by the bow shock and its evolution within the magnetosheath. Toward that end, we have integrated $\mathbf{j} \cdot \mathbf{E}'$ across the event, shown in the text label in Figure 3e.

[Figure 3 about here.]

As can be seen in Figure 2e, the $3\sigma$ events are distributed roughly uniformly throughout the turbulent sheath interval, so either an individual event survives this entire traversal or, more likely, it lasts some time and is replaced by an equivalent structure. Since the spacecraft is moving slowly with respect to the sheath flow, a time average is equivalent to a spatial average within the turbulent sheath. Thus the average energy conversion rate per unit volume in the magnetosheath is simply the sum of $\mathbf{j} \cdot \mathbf{E}'$ integrated across all the observed events divided by the total observation time $T_{obs}$, i.e.,

$$\mathcal{E} = \frac{1}{T_{obs}} \sum \int \mathbf{j} \cdot \mathbf{E}' \; dt \tag{1}$$

We assume for simplicity that the events are all locally planar current sheets and oriented perpendicular to a constant sheath flow. Then the volume of the sheath is proportional to the distance $L$ throughout which the exchange (1) is occurring, so the energy conversion rate per unit area, compared to the incident ram energy flux at the bow shock, is:

$$\frac{\mathcal{F}_L}{\mathcal{F}_{SW}} = \frac{(L/T_{obs}) \sum \int \mathbf{j} \cdot \mathbf{E}' \; dt}{V_{sw} \rho V_{sw}^2/2} \tag{2}$$

## 3 Results

We looked at 59 current structures that matched our $3\sigma$ of $< |\mathbf{j}| >$ selection criterion. These included 27 events with magnetic depressions/near nulls, as that in Figure 3 and possible electron velocity jets parallel to the reversing field as found in magnetic reconnection sites, 14 which appeared to be tangential discontinuities lacking a dip in $|\mathbf{B}|$ and with constant total pressure, 3 which resembled rotational discontinuities with constant magnetic field strength, 6 which were reminiscent of flux ropes with a peak in $|\mathbf{B}|$ and total pressure, 3 which resembled steepened ULF waves with trailing wavetrains and 6 others. This classification is based on a qualitative assessment of variations of the parameters by inspection of plots identical in format to Figure 3, and is shown in Table S1 of the Supporting Information for all events together with the individual energy conversion values. We have not attempted a detailed analysis of, e.g., the traditional $lmn$ geometry for each event; we provide the event details in the Supporting Information for use in future studies.

The 59 events have an average duration of 2.8s. Taken together, they make up only 3% of the roughly 90 minute quasi-parallel magnetosheath traversal in which they were observed. Based on our assumption that the events are planar, they thus fill $\sim 3\%$ of the volume of the magnetosheath. Can such a small volume process a significant amount of energy?

Figure 4 summarizes the energy conversion statistics for all the events. Most of the events (nearly 75%)) have positive integrated $\mathbf{j}\cdot\mathbf{E}'$ indicating that they convert field energy into particle energy on the average. Summing over all 59 events, Equation (2) reveals that the net conversion of $4.0\times10^{-9}$Ws/m$^3$ corresponds to $\sim 5\%$ of the incident solar wind ram energy flux. By way of comparison, the rise in electron enthalpy flux across the bow shock itself is $\sim 20\%$ of the ram energy flux, while the increase in electron enthalpy flux from just downstream of the bow shock (at 07:50 where $T_e \sim 40\,\text{eV}$) to the downstream edge of the quasi-parallel magnetosheath (at 06:45 where $T_e \sim 55\,\text{eV}$) represents $\sim 7.5\%$ of that same incident ram energy flux. These comparisons reveal that the isolated current events studied here are energetically comparable to both the heating at the bow shock itself and to the continued increase in electron temperature with downstream distance. We discuss below the caution that should be applied here, since

$\mathbf{j}\cdot\mathbf{E}'$ is the total energy conversion, including bulk flow, adiabatic compression and irreversible dissipation.

As a final note here, we have seen that these current events can have both positive and negative energy conversions. In terms of their overall impact on the energetics of the sheath, we have calculated the total energy processed by the events regardless of sign by summing $|\mathbf{j}\cdot\mathbf{E}'|$. This conversion is $8.9\times10^{-9}$Ws/m$^3$, corresponding to 11% of the incident ram energy flux.

[Figure 4 about here.]

## 4 Discussion

Our results show that isolated current structures within the magnetosheath downstream of the quasi-parallel bow shock convert electromagnetic field energy into particle energy at a rate that is comparable to the increase in electron enthalpy flux within the magnetosheath, and 25% of the change in that enthalpy flux occurring at the shock itself. If that conversion is all irreversible, this implies that roughly 20% of the electron heating from the solar wind to deep in the magnetosheath is (a) distributed throughout the magnetosheath and (b) localized in space to the most intense currents. However, the electro-fluid dynamics can't distinguish irreversible heating from reversible compression or accelerated flows. Recent work in the context of plasma turbulence (Matthaeus et al., 2020) has attempted to separate out these different energy reservoirs. They conclude that there is no direct correlation between the intense current sheets and their $\Pi-D$ measure of dissipation (Bandyopadhyay et al., 2020), although they do find that dissipation is highly spatially localized near to intense current events. We note in this context that most of our events, such as that shown in Figure 3, do not show significant temperature changes within them.

However, our goal here is simpler, namely to establish whether intense currents are significant in terms of the overall shock and sheath energetics. For the case studied here the total energy conversion (ignoring the sign) is approximately 11% of the ram energy flux incident at the bow shock. This is indicative of the incompleteness of the bow shock in thermalizing the incident ram energy and of the ongoing dissipation, redistribution, and relaxation of the plasma through the entire magnetosheath. Yet this specific energy conversion is mediated by only $\sim 3\%$ of the volume of the magnetosheath.

## 5 Conclusions

We have studied the exchange between particle and electromagnetic energy downstream of the quasi-parallel Earth's bow shock through the analysis of a traversal of the sub-solar magnetosheath by MMS. The interplanetary conditions were steady, and an unusually long interval of burst mode data was available. Our main conclusion is that thin current events or sheets, which are approximately 3 s in duration and thus occupy 3% of the magnetosheath volume, process nearly 11% of the bulk flow ram energy incident at the bow shock. In this example, that energy conversion was predominantly from field energy to particle energy. We are not able to determine whether that represents irreversible dissipation or reversible compressions (Matthaeus et al., 2020), nor the partition of that particle energy between electrons and ions. Nonetheless, our results show the importance of these isolated thin current structures in the energy processing that is initiated at the bow shock but continues far into the downstream region.

The region downstream of a quasi-parallel shock is well-known to be turbulent (Lucek et al., 2005; Burgess et al., 2005) which promotes the formation of thin current structures. The fluctuation levels, and hence current sheet intensities, downstream of the quasi-perpendicular bow shock are much less. This can even be seen in the first third of Figure 1(a-f) before the interplanetary field turned to more quasi-parallel geometries. These regions show less evolution in density compression or temperature, suggesting that the binding of the particles and fields by the perpendicular geometry promotes more rapid energy exchange. There may nonetheless be subtle changes within individual particle populations as, e.g., anisotropy-driven instabilities relax these populations toward thermal equilibrium. This could be productively explored in a similar future study of this kind. Upstream disturbances such as hot flow anomalies and foreshock bubbles, together with higher levels of interplanetary turbulence, may also lead to higher levels of magnetosheath turbulence which again could promote more numerous and intense current sheets even under quasi-perpendicular geometries.

### Acknowledgments

Artemis and Wind data were drawn from the SPDF/CDAWEB repository (`https://cdaweb.gsfc.nasa.gov/index.html/`). We gratefully acknowledge the respective instrument teams and archive curators. MMS data can be found at the MMS public Science Data Center (`https://lasp.colorado.edu/mms/sdc/public/`). All the data analysis and graphics were performed using the opensource QSAS Science Analysis System (`https://sourceforge.net/projects/qsas/`). This work was supported by NASA Award 80NSSC19K0849 together with NASA MMS contracts to the instrument teams. IG is supported by a Royal Society URF.

## References

Bandyopadhyay, R., Matthaeus, W. H., Parashar, T. N., Yang, Y., Chasapis, A., Giles, B. L., … Burch, J. L. (2020, June). Statistics of Kinetic Dissipation in the Earth's Magnetosheath: MMS Observations. *Phys. Rev. Lett.*, *124*(25), 255101. doi: 10.1103/PhysRevLett.124.255101

Bessho, N., Chen, L. J., Wang, S., Hesse, M., Wilson, I., L. B., & Ng, J. (2020, September). Magnetic reconnection and kinetic waves generated in the Earth's quasi-parallel bow shock. *Phys. Plasmas*, *27*(9), 092901. doi: 10.1063/5.0012443

Burch, J. L., Moore, T. E., Torbert, R. B., & Giles, B. L. (2016, March). Magnetospheric Multiscale Overview and Science Objectives. *Space Sci. Rev.*, *199*, 5-21. doi: 10.1007/s11214-015-0164-9

Burch, J. L., Torbert, R. B., Phan, T. D., Chen, L. J., Moore, T. E., Ergun, R. E., … Chandler, M. (2016, June). Electron-scale measurements of magnetic reconnection in space. *Science*, *352*, aaf2939. doi: 10.1126/science.aaf2939

Burgess, D., Lucek, E. A., Scholer, M., Bale, S. D., Balikhin, M. A., Balogh, A., … Walker, S. N. (2005, June). Quasi-parallel Shock Structure and Processes. *Sp. Sci. Rev.*, *118*(1-4), 205-222. doi: 10.1007/s11214-005-3832-3

Burgess, D., & Scholer, M. (2015). *Collisionless Shocks in Space Plasmas.* Cambridge University Press.

Chanteur, G. (1998, January). Spatial Interpolation for Four Spacecraft: Theory. *ISSI Scientific Reports Series*, *1*, 349-370.

Dunlop, M. W., & Eastwood, J. P. (2008, January). The Curlometer and Other Gradient Based Methods. *ISSI Scientific Reports Series*, *8*, 17-26.

Eastwood, J. P., Lucek, E. A., Mazelle, C., Meziane, K., Narita, Y., Pickett, J., & Treumann, R. A. (2005, June). The Foreshock. *Sp. Sci. Rev.*, *118*(1-4), 41-94. doi: 10.1007/s11214-005-3824-3

Ergun, R. E., Tucker, S., Westfall, J., Goodrich, K. A., Malaspina, D. M., Summers, D., … Cully, C. M. (2016, March). The Axial Double Probe and Fields Signal Processing for the MMS Mission. *Space Sci. Rev.*, *199*, 167-188. doi: 10.1007/s11214-014-0115-x

Gingell, I., Schwartz, S. J., Eastwood, J. P., Burch, J. L., Ergun, R. E., Fuselier, S., … Wilder, F. (2019, February). Observations of Magnetic Reconnection in the Transition Region of Quasi-Parallel Shocks. *Geophys. Res. Lett.*, *46*(3), 1177-1184. doi: 10.1029/2018GL081804

Gingell, I., Schwartz, S. J., Eastwood, J. P., Stawarz, J. E., Burch, J. L., Ergun, R. E., … Wilder, F. (2020, January). Statistics of Reconnecting Current Sheets in the Transition Region of Earth's Bow Shock. *J. Geophys. Res.*, *125*(1), e27119. doi: 10.1029/2019JA027119

Krasnoselskikh, V., Balikhin, M., Walker, S. N., Schwartz, S., Sundkvist, D., Lobzin, V., … Comisel, H. (2013, October). The Dynamic Quasiperpendicular Shock: Cluster Discoveries. *Sp. Sci. Rev.*, *178*(2-4), 535-598. doi: 10.1007/s11214-013-9972-y

Kucharek, H., Möbius, E., Li, W., Farrugia, C. J., Popecki, M. A., Galvin, A. B., … Bochsler, P. A. (2003, October). On the source and acceleration of energetic $He^+$: A long-term observation with ACE/SEPICA. *J. Geophys. Res.*, *108*(A10), 8040. doi: 10.1029/2003JA009938

Lindqvist, P.-A., Olsson, G., Torbert, R. B., King, B., Granoff, M., Rau, D., … Tucker, S. (2016, March). The Spin-Plane Double Probe Electric Field Instrument for MMS. *Space Sci. Rev.*, *199*, 137-165. doi: 10.1007/s11214-014-0116-9

Lucek, E. A., Constantinescu, D., Goldstein, M. L., Pickett, J., Pinçon, J. L., Sahraoui, F., … Walker, S. N. (2005, June). The Magnetosheath. *Sp. Sci. Rev.*, *118*(1-4), 95-152. doi: 10.1007/s11214-005-3825-2

Matthaeus, W. H., Yang, Y., Wan, M., Parashar, T. N., Bandyopadhyay, R., Chasapis, A. r., … Valentini, F. (2020, March). Pathways to Dissipation in Weakly Collisional Plasmas. *Astrophys. J.*, *891*(1), 101. doi: 10.3847/1538-4357/ab6d6a

Phan, T. D., Eastwood, J. P., Shay, M. A., Drake, J. F., Sonnerup, B. U. Ö., Fujimoto, M., … Magnes, W. (2018, May). Electron magnetic reconnection without ion coupling in Earth's turbulent magnetosheath. *Nature*, *557*(7704), 202-206. doi: 10.1038/s41586-018-0091-5

Pollock, C., Moore, T., Jacques, A., Burch, J., Gliese, U., Saito, Y., . . . others (2016, March). Fast Plasma Investigation for Magnetospheric Multiscale. *Space Sci. Rev.*, *199*, 331-406. doi: 10.1007/s11214-016-0245-4

Retinò, A., Sundkvist, D., Vaivads, A., Mozer, F., André, M., & Owen, C. J. (2007, April). In situ evidence of magnetic reconnection in turbulent plasma. *Nat. Phys.*, *3*(4), 236-238. doi: 10.1038/nphys574

Russell, C. T., Anderson, B. J., Baumjohann, W., Bromund, K. R., Dearborn, D., Fischer, D., . . . Richter, I. (2016, March). The Magnetospheric Multiscale Magnetometers. *Space Sci. Rev.*, *199*, 189-256. doi: 10.1007/s11214-014-0057-3

Schwartz, S. J. (1998, January). Shock and Discontinuity Normals, Mach Numbers, and Related Parameters. *ISSI Scientific Reports Series*, *1*, 249-270.

Schwartz, S. J. (2006, June). Shocks: Commonalities in Solar-Terrestrial Chains. *Sp. Sci. Rev.*, *124*(1-4), 333-344. doi: 10.1007/s11214-006-9093-y

Schwartz, S. J., Zweibel, E. G., & Goldman, M. (2013, October). Microphysics in Astrophysical Plasmas. *Sp. Sci. Rev.*, *178*(2-4), 81-99. doi: 10.1007/s11214-013-9975-8

Scudder, J. D., Mangeney, A., Lacombe, C., Harvey, C. C., Wu, C. S., & Anderson, R. R. (1986, October). The resolved layer of a collisionless, high $\beta$, supercritical, quasi-perpendicular shock wave, 3. Vlasov electrodynamics. *J. Geophys. Res.*, *91*(A10), 11075-11098. doi: 10.1029/JA091iA10p11075

Slavin, J. A., & Holzer, R. E. (1981, December). Solar wind flow about the terrestrial planets, 1. Modeling bow shock position and shape. *J. Geophys. Res.*, *86*(A13), 11401-11418. doi: 10.1029/JA086iA13p11401

Stawarz, J. E., Eastwood, J. P., Phan, T. D., Gingell, I. L., Shay, M. A., Burch, J. L., . . . Franci, L. (2019, June). Properties of the Turbulence Associated with Electron-only Magnetic Reconnection in Earth's Magnetosheath. *Astrophys. J. Lett.*, *877*(2), L37. doi: 10.3847/2041-8213/ab21c8

Stone, R. G., & Tsurutani, B. T. (1985, January). Collisionless shocks in the heliosphere. A tutorial review. *Washington DC American Geophysical Union Geophysical Monograph Series*, *34*. doi: 10.1029/GM034

Swisdak, M., Drake, J. F., Price, L., Burch, J. L., Cassak, P. A., & Phan, T. D.

(2018, June). Localized and Intense Energy Conversion in the Diffusion Region of Asymmetric Magnetic Reconnection. *Geophys. Res. Lett.*, *45*(11), 5260-5267. doi: 10.1029/2017GL076862

Torbert, R. B., Russell, C. T., Magnes, W., Ergun, R. E., Lindqvist, P.-A., LeContel, O., … Lappalainen, K. (2016, March). The FIELDS Instrument Suite on MMS: Scientific Objectives, Measurements, and Data Products. *Space Sci. Rev.*, *199*, 105-135. doi: 10.1007/s11214-014-0109-8

Tsurutani, B. T., & Stone, R. G. (1985, January). Collisionless shocks in the heliosphere: Reviews of current research. *Washington DC American Geophysical Union Geophysical Monograph Series*, *35*. doi: 10.1029/GM035

Wang, S., Chen, L.-J., Bessho, N., Hesse, M., Wilson, L. B., Giles, B., … Burch, J. L. (2019, January). Observational Evidence of Magnetic Reconnection in the Terrestrial Bow Shock Transition Region. *Geophys. Res. Lett.*, *46*(2), 562-570. doi: 10.1029/2018GL080944

Wilder, F. D., Ergun, R. E., Burch, J. L., Ahmadi, N., Eriksson, S., Phan, T. D., … Khotyaintsev, Y. V. (2018, August). The Role of the Parallel Electric Field in Electron-Scale Dissipation at Reconnecting Currents in the Magnetosheath. *J. Geophys. Res.*, *123*(8), 6533-6547. doi: 10.1029/2018JA025529

Zenitani, S., Hesse, M., Klimas, A., & Kuznetsova, M. (2011, May). New Measure of the Dissipation Region in Collisionless Magnetic Reconnection. *Phys. Rev. Lett.*, *106*(19), 195003. doi: 10.1103/PhysRevLett.106.195003

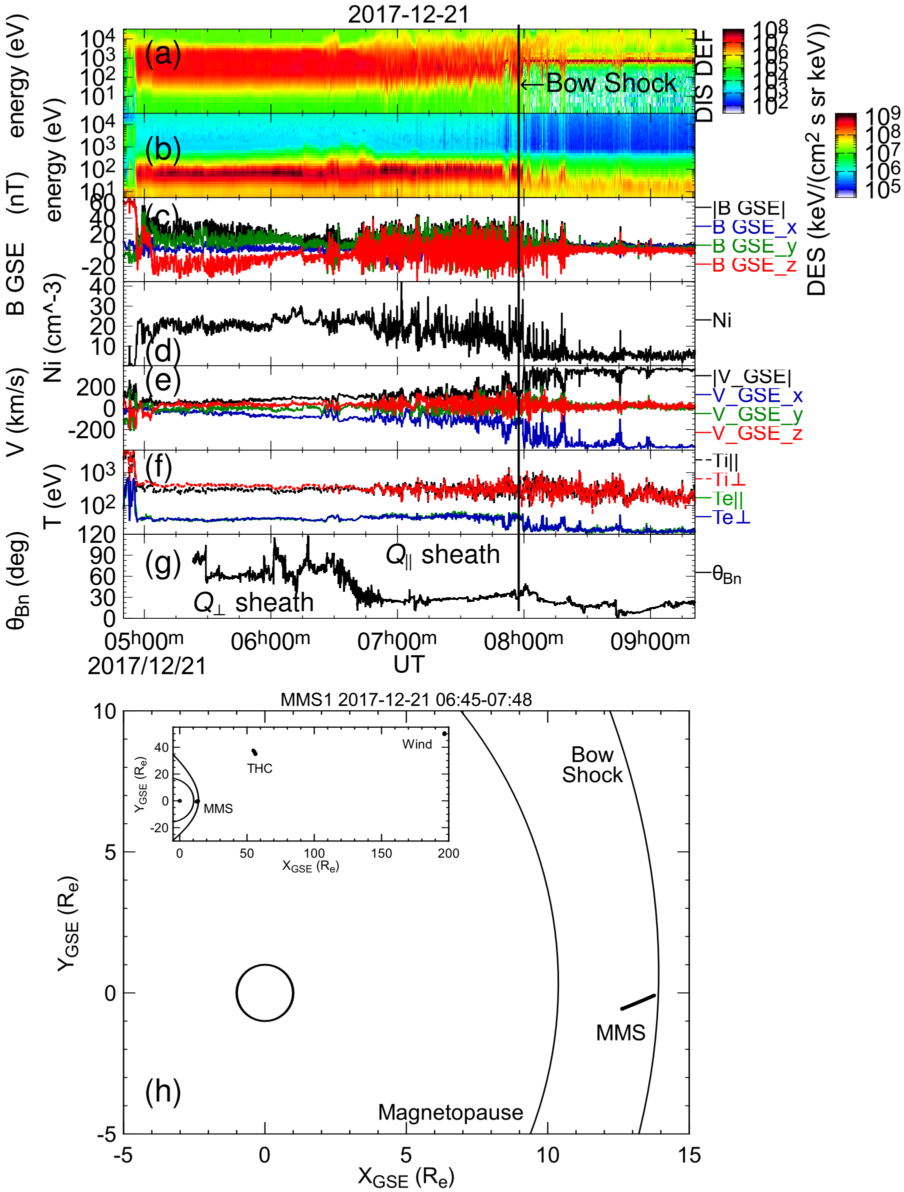


**Figure 1.** Top: Overview of the magnetosheath crossing by MMS1 on 2017/12/21. Ion (a) and electron (b) differential energy fluxes, (c) magnetic field in GSE, (d) ion density (e) ion flow velocity (f) electron and ion temperatures parallel and perpendicular to the local magnetic field and (g) angle between the interplanetary magnetic field (lagged in time from the WIND spacecraft) and the normal to a model of the Earth's bow shock. Bottom: (h) Trajectory of MMS showing an essentially sub-solar traversal of the magnetosheath together with (inset) the locations of THC (Artemis) and Wind spacecraft which were used to determine the lagged interplanetary plasma conditions. The four MMS spacecraft were separated by ∼25km.

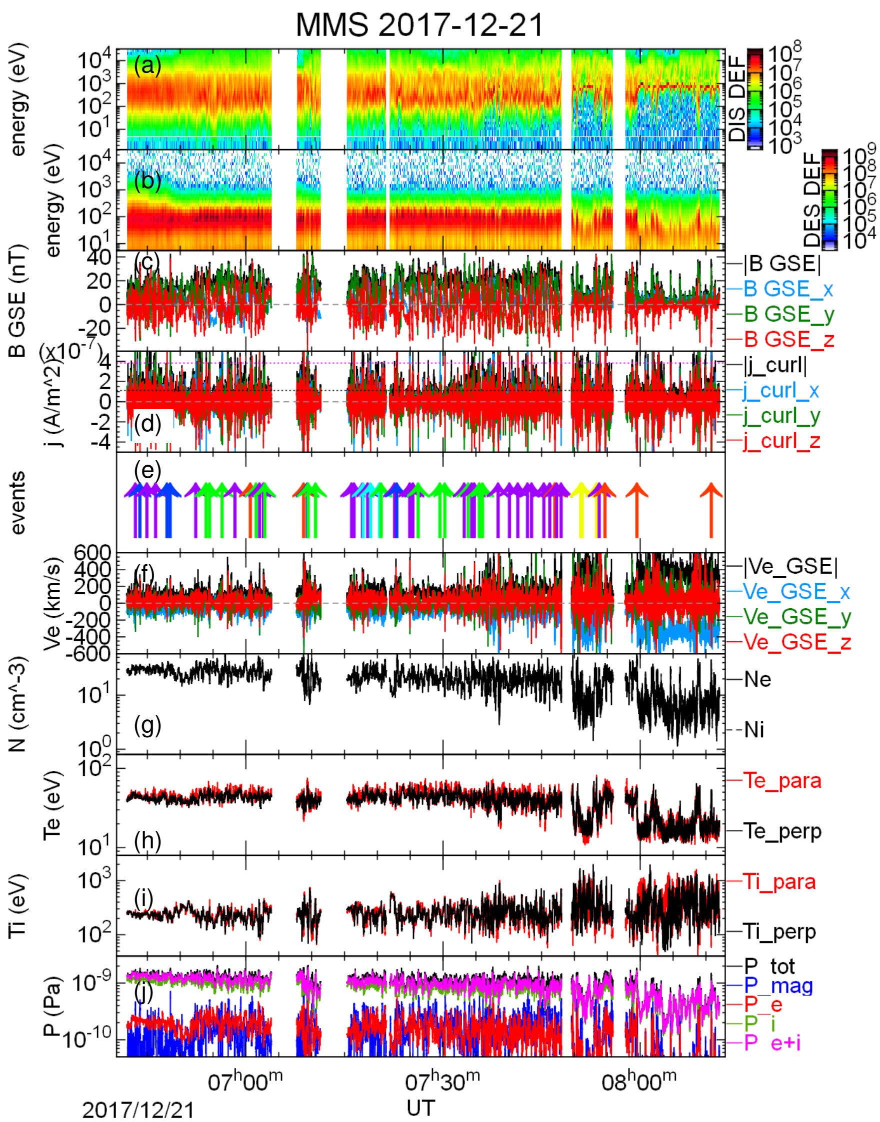


**Figure 2.** Overview of the burst-mode data from the MMS quasi-parallel sheath crossing observed on 2017-12-21. All data are from MMS1 except the current density. Ion (a) and electron (b) differential energy fluxes in keV/(cm$^2$ s sr keV) (c) magnetic field in GSE, (d) electric current density calculated from a curlometer technique. Dotted lines show the $1\sigma$ and $3\sigma$ $|\mathbf{j}|$ levels (e) selected events with $|\mathbf{j}| > 3\sigma$, color coded by probable type of current structure (see text and Figure 4 below) (f) electron bulk flow velocity (g) electron and ion plasma densities (indistinguishable on this scale) (h) electron and (i) ion temperatures parallel and perpendicular to the local magnetic field and (j) plasma, field and total pressure.

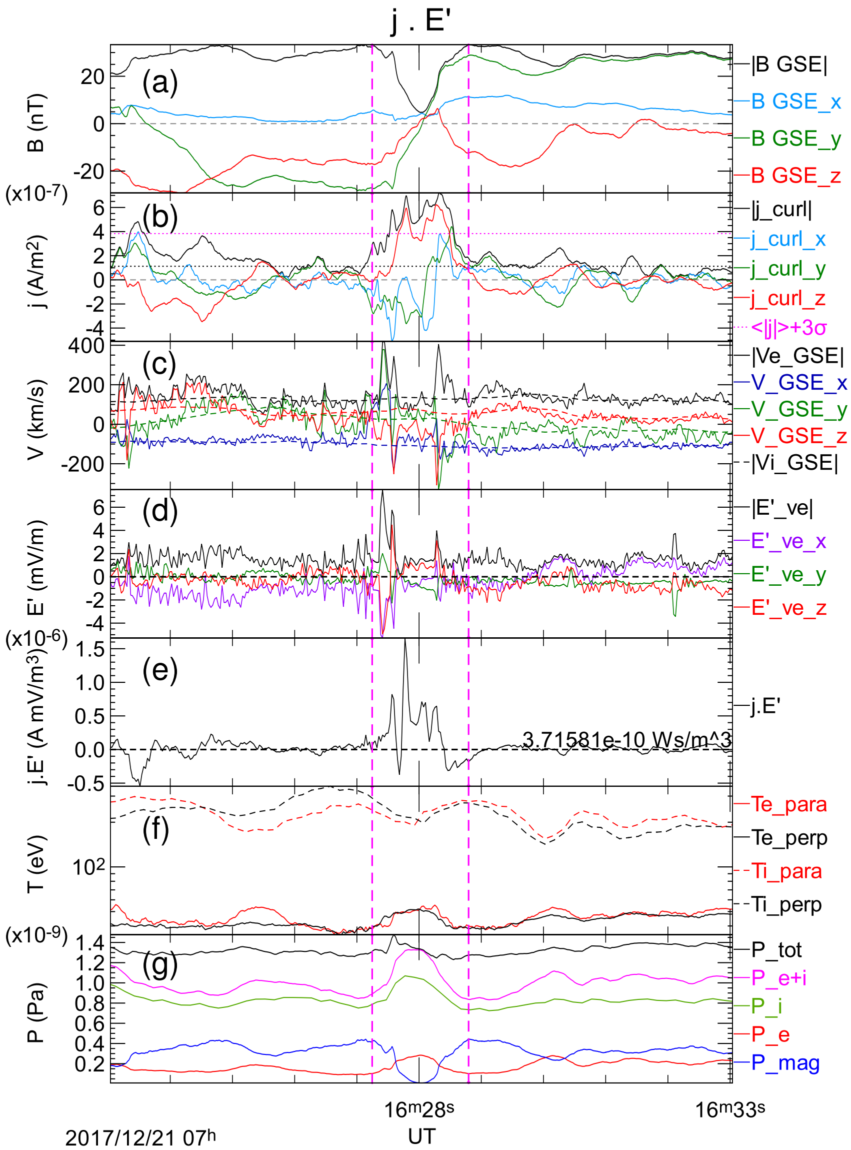


**Figure 3.** An example of the current sheets/structures selected for this study. Data from MMS1 except in (b) and (e) Top to bottom (a) magnetic field in GSE (b) current density $\mathbf{j}$ in GSE calculated via the curlometer method (c) electron (solid) and ion (dashed) bulk flow velocities (d) DC electric field transformed into the electron flow frame (e) energy conversion rate $\mathbf{j}\cdot\mathbf{E}'$ based on $\mathbf{E}'$ calculated at the barycenter of the four spacecraft tetrahedron (f) electron (solid) and ion (dashed) temperatures parallel (red) and perpendicular (black) to the instantaneous magnetic field (g) magnetic, particle, and total plasma pressure. Note the current density rises above the dashed $3\sigma$ line in panel (b), and the region surrounding this selected manually as the full event delineated by dashed vertical magenta lines. The integral of $\mathbf{j}\cdot\mathbf{E}'$ over the event is shown in panel (e).

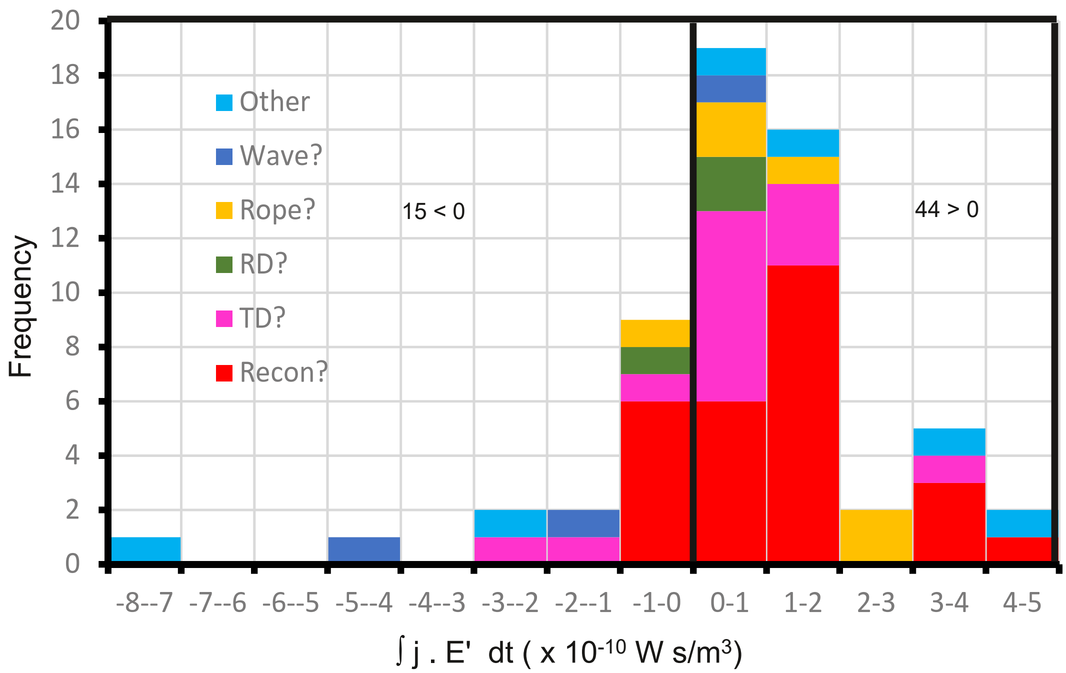


**Figure 4.** Statistics of the integrated energy conversion $\int \mathbf{j} \cdot \mathbf{E}' \, dt$ for the 59 events in this study, broken down by the apparent type of the event (see text).

# Energy Conversion within Current Sheets in the Earth's Quasi-parallel Magnetosheath: Supporting Information

Steven J Schwartz[1*†], Harald Kucharek[2], Charles J Farrugia[2], K.J. Trattner[1], Imogen Gingell[3], Robert Ergun[1], Robert Strangeway[4], Daniel Gershman[5]

[1]Laboratory for Atmospheric and Space Physics, CU Boulder, Boulder, CO

[2]University of New Hampshire, Durham, NH

[3]Physics and Astronomy, University of Southampton, Southampton, UK

[4]UCLA, Los Angeles, CA

[5]Goddard Space Flight Center, Greenbelt, MD

Manuscript date November 24, 2020

**Contents of this file**

1. Figure S1
2. Table S1

**Additional Supporting Information (Files uploaded separately)**

1. Caption for Dataset S1

**Introduction**

This Supporting Information contains a figure illustrating the method by which Wind plasma and magnetic field data were lagged to the location of the MMS spacecraft. It also includes a zip archive of plots in the same format as Figure 3 of the main paper for each of the 59 events used in the study. Some details for all the events are provided in Table S1.

**Figure S1.** Comparison of data from MMS1 after smoothing (thin) with data from the Wind spacecraft lagged by $23^m 10^s$ for the magnetosheath traversal studied in the main paper. This lag was determined through the intermediary step of data from the Themis-C (Artemis) spacecraft (not shown) which was closer upstream of MMS (see Figure 1h of the main paper) but which lacks instrumentation designed for resolving the solar wind. Magnetic field magnitude (a) and GSE components (b), (c) angle $\theta_{Bn}$ between the laggeed Wind magnetic field and the shock normal based on a model scaled to fit the MMS shock crossing, (d) magnetic field clock angle ($\tan^{-1} B_y/B_z$); at the subsolar point, magnetic coplanarity preserves this angle from upstream to downstream which enables a comparison between MMS in the magnetosheath and the lagged Wind values. Note the good fit between MMS and Wind across the entire plot range. Solar wind speed [(e),(g)] and GSE velocity components [(f),(h)] for protons/ions and electrons respectively. (i) number density, (j) electron temperatures and (k) ion temperatures. The interplanetary conditions were steady after 06:45 as can be seen in the Wind plasma and field parameters. The dashed vertical magenta lines indicate the interval of Wind data used to deduce the underlying interplanetary conditions and shock parameters.

**Table S1** List of all 59 current events studied in the main paper, including start and end times, value of the integrated energy conversion, and category of qualitative nature of the event. Also shown is the figure index number of each event; plots are available in the archive (Data Set S1).

**Data Set S1.** DS01 is a zip archive containing plots identical in format to that of Figure 3 in the main paper for each of the 59 events used in this study.

*Laboratory for Atmospheric and Space Physics, CU Boulder, Boulder, CO

†Also Emeritus Professor, Imperial College London


0094-8276/20/$5.00

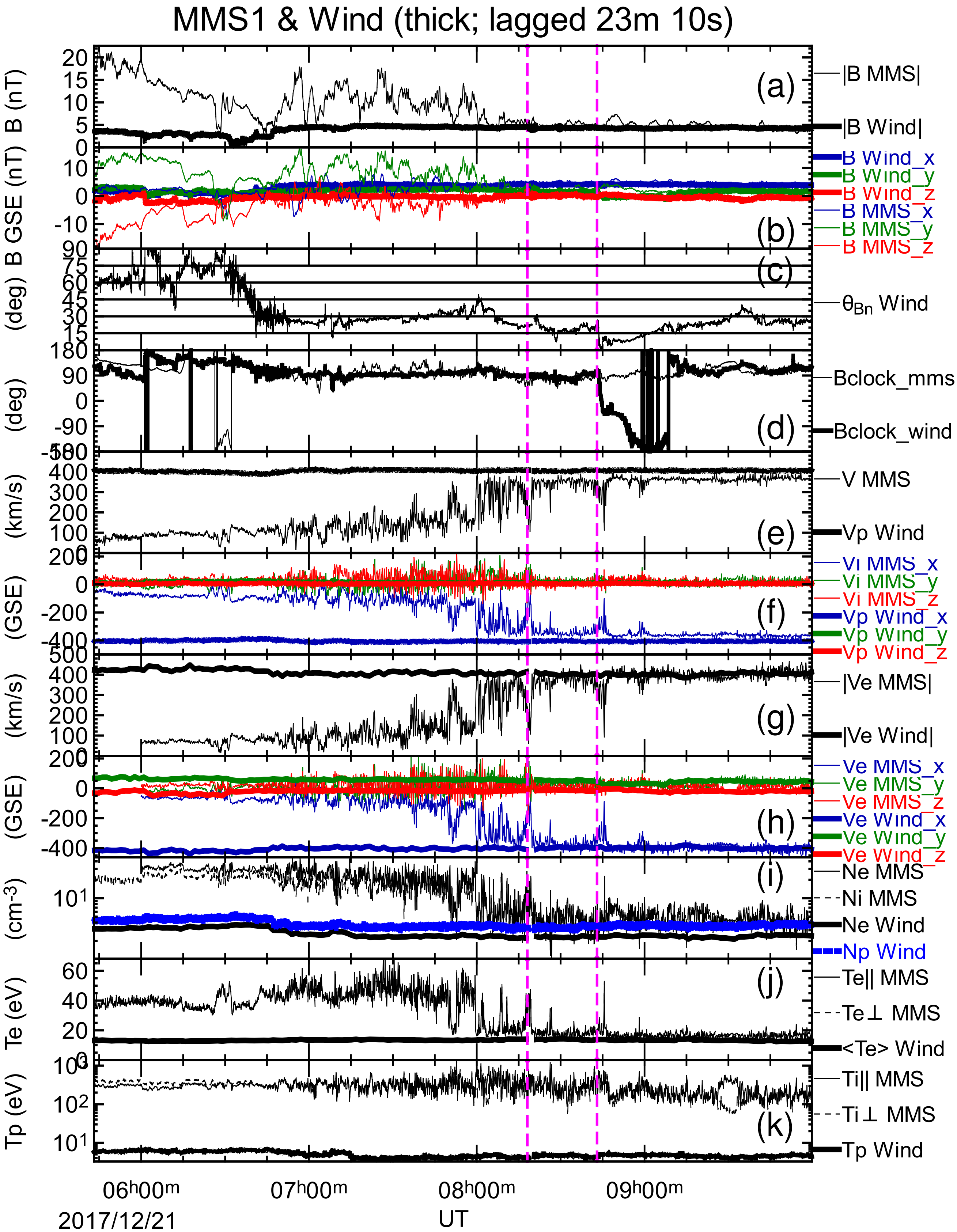
MMS1 & Wind (thick; lagged 23m 10s)
B (nT)
B GSE (nT)
(deg)
(deg)
(km/s)
(GSE)
(km/s)
(GSE)
(cm-3)
Te (eV)
Tp (eV)
(a)
(b)
(c)
(d)
(e)
(f)
(g)
(h)
(i)
(j)
(k)
|B MMS|
|B Wind|
B Wind_x
B Wind_y
B Wind_z
B MMS_x
B MMS_y
B MMS_z
θBn Wind
Bclock_mms
Bclock_wind
V MMS
Vp Wind
Vi MMS_x
Vi MMS_y
Vi MMS_z
Vp Wind_x
Vp Wind_y
Vp Wind_z
|Ve MMS|
|Ve Wind|
Ve MMS_x
Ve MMS_y
Ve MMS_z
Ve Wind_x
Ve Wind_y
Ve Wind_z
Ne MMS
Ni MMS
Ne Wind
Np Wind
Te|| MMS
Te⊥ MMS
<Te> Wind
Ti|| MMS
Ti⊥ MMS
Tp Wind
06h00m
07h00m
08h00m
09h00m
2017/12/21
UT

**Figure S1.** Comparison of data from MMS1 after smoothing (thin) with data from the Wind spacecraft lagged by $23^m10^s$ for the magnetosheath traversal studied in the main paper. This lag was determined through the intermediary step of data from the Themis-C (Artemis) spacecraft (not shown) which was closer upstream of MMS (see Figure 1h of the main paper) but which lacks instrumentation designed for resolving the solar wind. Magnetic field magnitude (a) and GSE components (b), (c) angle $\theta_{Bn}$ between the laggeed Wind magnetic field and the shock normal based on a model scaled to fit the MMS shock crossing, (d) magnetic field clock angle ($\tan^{-1} B_y/B_z$); at the subsolar point, magnetic coplanarity preserves this angle from upstream to downstream which enables a comparison between MMS in the magnetosheath and the lagged Wind values. Note the good fit between MMS and Wind across the entire plot range. Solar wind speed [(e),(g)] and GSE velocity components [(f),(h)] for protons/ions and electrons respectively. (i) number density, (j) electron temperatures and (k) ion temperatures. The interplanetary conditions were steady after 06:45 as can be seen in the Wind plasma and field parameters. The dashed vertical magenta lines indicate the interval of Wind data used to deduce the underlying interplanetary conditions and shock parameters.

**Table S1.** Current Events 2017-12-21 Magnetosheath

| Fig no | Start time | End time | $\int \mathbf{j} \cdot \mathbf{E}' dt$[1] | Cat[2] |
|---|---|---|---|---|
| 1 | 2017-12-21T06:43:11.102450 | 2017-12-21T06:43:11.877474 | 1.9 | 1 |
| 2 | 2017-12-21T06:43:52.343473 | 2017-12-21T06:43:55.064668 | 1.17 | 2 |
| 3 | 2017-12-21T06:44:56.381627 | 2017-12-21T06:44:57.983343 | 1.23 | 1 |
| 5 | 2017-12-21T06:45:33.199240 | 2017-12-21T06:45:35.214302 | 0.1 | 2 |
| 6 | 2017-12-21T06:46:15.614235 | 2017-12-21T06:46:16.527040 | 0.58 | 1 |
| 7 | 2017-12-21T06:47:59.133220 | 2017-12-21T06:48:01.664965 | 2.54 | 2 |
| 8 | 2017-12-21T06:48:28.317135 | 2017-12-21T06:48:31.003884 | 0.9 | 2 |
| 9 | 2017-12-21T06:52:21.951134 | 2017-12-21T06:52:24.310651 | -0.152 | 1 |
| 10 | 2017-12-21T06:53:56.435223 | 2017-12-21T06:53:57.554702 | 0.44 | 4 |
| 11 | 2017-12-21T06:54:27.902201 | 2017-12-21T06:54:30.588950 | 0.53 | 4 |
| 12 | 2017-12-21T06:56:22.662678 | 2017-12-21T06:56:23.954384 | -0.52 | 4 |
| 13 | 2017-12-21T06:58:19.564296 | 2017-12-21T06:58:20.942117 | -0.69 | 1 |
| 14 | 2017-12-21T07:00:40.167183 | 2017-12-21T07:01:00.421140 | 1.1 | 6 |
| 15 | 2017-12-21T07:01:33.216487 | 2017-12-21T07:01:34.318743 | 0.36 | 4 |
| 16 | 2017-12-21T07:02:04.402691 | 2017-12-21T07:02:05.229383 | 1.37 | 1 |
| 17 | 2017-12-21T07:02:40.081670 | 2017-12-21T07:02:41.511159 | 1.94 | 1 |
| 18 | 2017-12-21T07:02:52.157496 | 2017-12-21T07:02:53.173638 | 0.2 | 4 |
| 21 | 2017-12-21T07:08:46.908785 | 2017-12-21T07:08:49.776373 | 0.78 | 6 |
| 22 | 2017-12-21T07:09:19.872507 | 2017-12-21T07:09:23.876797 | 2.02 | 2 |
| 23 | 2017-12-21T07:09:28.270908 | 2017-12-21T07:09:29.321496 | 0.23 | 4 |
| 24 | 2017-12-21T07:10:36.002549 | 2017-12-21T07:10:38.585962 | 1.28 | 4 |
| 25 | 2017-12-21T07:16:05.172733 | 2017-12-21T07:16:06.154430 | 0.41 | 1 |
| 26 | 2017-12-21T07:16:27.245998 | 2017-12-21T07:16:28.796046 | 3.72 | 1 |
| 27 | 2017-12-21T07:17:43.854349 | 2017-12-21T07:17:44.629373 | 0.89 | 1 |
| 28 | 2017-12-21T07:17:50.581643 | 2017-12-21T07:17:53.251170 | 0.61 | 3 |
| 29 | 2017-12-21T07:18:31.498364 | 2017-12-21T07:18:33.168971 | 0.45 | 1 |
| 30 | 2017-12-21T07:18:58.390998 | 2017-12-21T07:18:59.665481 | -0.98 | 3 |
| 31 | 2017-12-21T07:20:20.010681 | 2017-12-21T07:20:23.351895 | 0.94 | 3 |
| 32 | 2017-12-21T07:20:34.226997 | 2017-12-21T07:20:46.317370 | 3.63 | 4 |
| 33 | 2017-12-21T07:22:37.121167 | 2017-12-21T07:22:39.377348 | 1.22 | 1 |
| 34 | 2017-12-21T07:22:57.601541 | 2017-12-21T07:23:02.329187 | -0.49 | 2 |
| 35 | 2017-12-21T07:24:55.848104 | 2017-12-21T07:24:57.914835 | 3.37 | 1 |
| 36 | 2017-12-21T07:25:24.766692 | 2017-12-21T07:25:26.747308 | 3.17 | 1 |
| 37 | 2017-12-21T07:26:12.637723 | 2017-12-21T07:26:16.254501 | -2.8 | 4 |
| 38 | 2017-12-21T07:29:31.054944 | 2017-12-21T07:29:33.621134 | 1.87 | 4 |
| 39 | 2017-12-21T07:30:16.032762 | 2017-12-21T07:30:19.391199 | -1.21 | 4 |
| 40 | 2017-12-21T07:33:13.268205 | 2017-12-21T07:33:15.455494 | 1.21 | 1 |
| 41 | 2017-12-21T07:33:49.904569 | 2017-12-21T07:33:50.834597 | 0.62 | 4 |
| 42 | 2017-12-21T07:34:21.453782 | 2017-12-21T07:34:23.933858 | 4.3 | 1 |
| 43 | 2017-12-21T07:34:45.285519 | 2017-12-21T07:34:46.508334 | 0.17 | 1 |
| 44 | 2017-12-21T07:35:30.679710 | 2017-12-21T07:35:34.451492 | 0.61 | 4 |
| 45 | 2017-12-21T07:36:00.294907 | 2017-12-21T07:36:02.912766 | 1.54 | 4 |
| 46 | 2017-12-21T07:38:22.491826 | 2017-12-21T07:38:27.038633 | 1.32 | 1 |
| 47 | 2017-12-21T07:40:05.802071 | 2017-12-21T07:40:08.514655 | 1.88 | 1 |
| 48 | 2017-12-21T07:41:22.537474 | 2017-12-21T07:41:24.018631 | 1.38 | 1 |
| 49 | 2017-12-21T07:42:51.235817 | 2017-12-21T07:42:55.059268 | 1.63 | 1 |
| 50 | 2017-12-21T07:43:28.342479 | 2017-12-21T07:43:29.892527 | -0.66 | 1 |
| 51 | 2017-12-21T07:45:20.044627 | 2017-12-21T07:45:22.128580 | 0.6 | 1 |
| 52 | 2017-12-21T07:46:14.301983 | 2017-12-21T07:46:18.917680 | -0.38 | 1 |
| 53 | 2017-12-21T07:47:00.418123 | 2017-12-21T07:47:03.931565 | -2.08 | 6 |
| 54 | 2017-12-21T07:47:16.625850 | 2017-12-21T07:47:17.745329 | -0.74 | 1 |
| 55 | 2017-12-21T07:47:58.054875 | 2017-12-21T07:47:59.639369 | 1.5 | 1 |
| 56 | 2017-12-21T07:50:56.576075 | 2017-12-21T07:50:59.331715 | -1.19 | 5 |
| 57 | 2017-12-21T07:51:10.838279 | 2017-12-21T07:51:11.682194 | 0.52 | 5 |
| 58 | 2017-12-21T07:53:20.482260 | 2017-12-21T07:53:22.945113 | -4.62 | 5 |
| 59 | 2017-12-21T07:53:45.277912 | 2017-12-21T07:53:47.361865 | -0.47 | 1 |
| 60 | 2017-12-21T07:54:37.853686 | 2017-12-21T07:54:48.704020 | 3.71 | 6 |
| 61 | 2017-12-21T07:59:30.267560 | 2017-12-21T07:59:33.806836 | -7.52 | 6 |
| 62 | 2017-12-21T08:10:49.259706 | 2017-12-21T08:10:51.429773 | 4.64 | 6 |

[1] in $10^{-10} Ws/m^3$

[2] 1 Recon; 2 Rope; 3 RD; 4 TD; 5 Wave; 6 other